Supplementary Information Appendix: Global Evaluation of Biofuel Potential from Microalgae

Jeffrey W. Moody[a], Christopher M. McGinty[b], Jason C. Quinn[a1]
[a]Mechanical & Aerospace Engineering, Utah State University, Logan, Utah, USA, 84322
[b]Departemtn of Wildland Resources, Utah State University, Logan, Utah, USA, 84322
[1]author for correspondence: Mechanical & Aerospace Engineering, 4130 Old Main Hill, Utah State University, Logan, Utah, USA, 84322, Phone: 435-797-0341, Email: Jason.Quinn@usu.edu

1. Simulation Architecture

The work outlined is based on the integration of a validated bulk growth model with historical meteorological data with results reduced using ArcGIS. The simulation architecture is presented in Fig. S1.

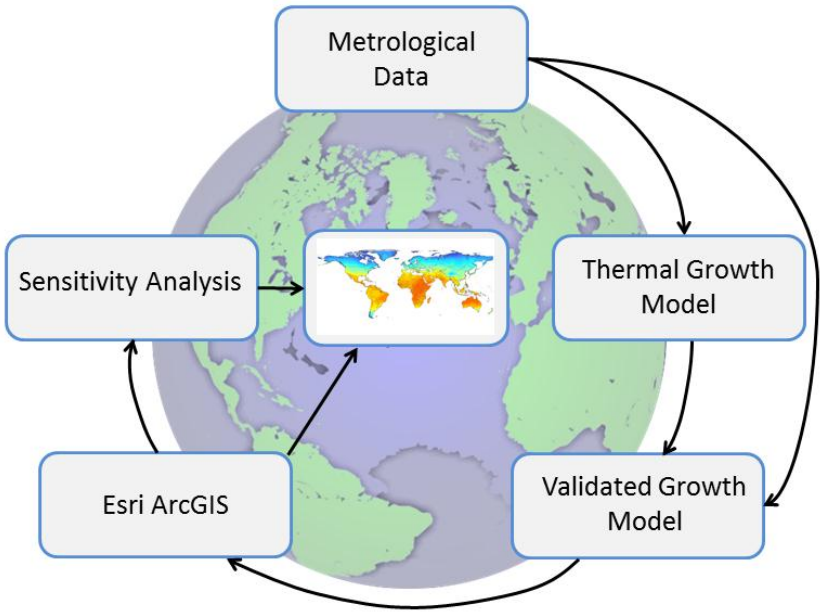

Fig. S1: Simulation architecture illustrating the use of a thermal and biological growth model as the foundation for a global map of the lipid productivity based on simulation with hourly historical meteorological data from 4,388 global locations.

2. Reactor Configuration and Operation

Model validation was done utilizing data from Solix generation 3 photobioreactors. A schematic of the overall geometry is presented in Fig. S2. The Solix reactor test bed was located in Fort Collins, Colorado adjacent to the Engines and Energy Conversion laboratory at Colorado State University. The

basin measures 3 meters by 18 meters and has sixteen reactors with dimensions detailed in Fig. S2. The outer most reactors receive more light and grow at a slightly elevated rate and were not included in the data set used for validation. The system was operated in two groups of 8 reactors. Growth was monitored continuously in one of the eight reactors and manual samples were taken from all reactors to verify uniform growth.

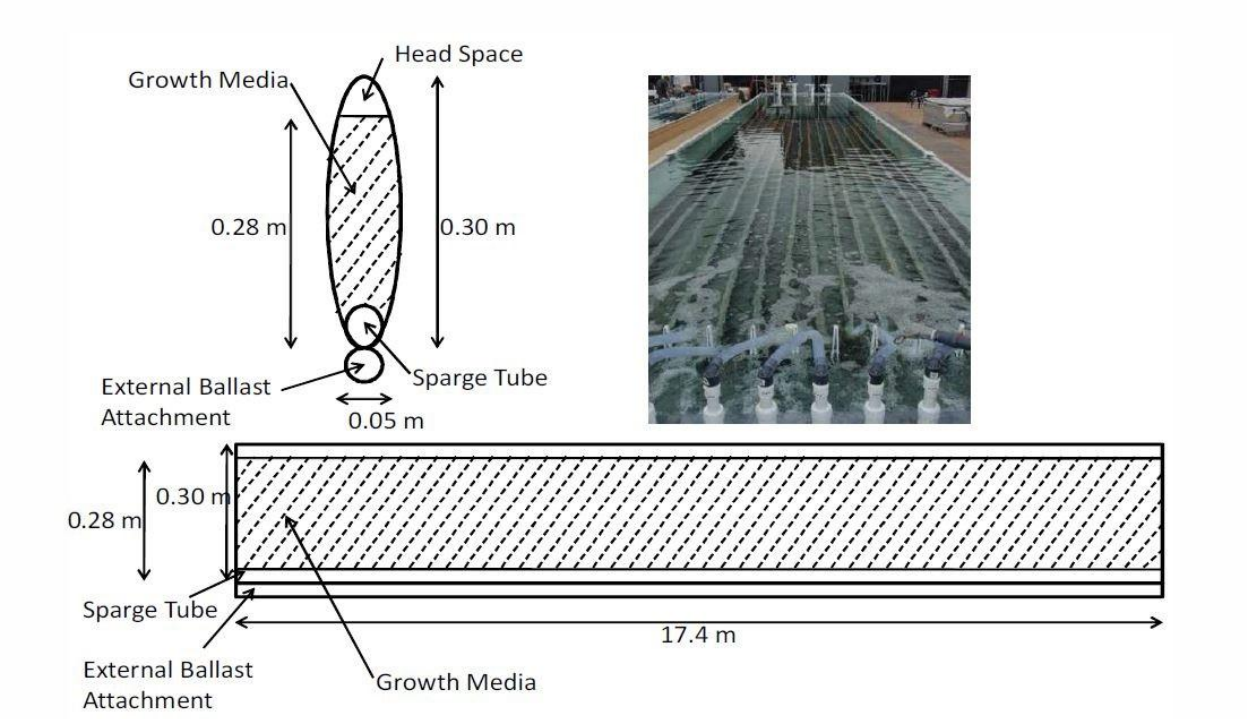

Fig. S2: Diagram and photograph of the Generation 3 Solix photobioreactor used to validate bulk growth model. Reactors are evenly spaced in a structural/thermal water basin in Fort Collins, Colorado, USA.

Reactors were harvested as a group. All of the culture was removed from the reactors, mixed for homogeneity and the required inocula were removed. The remainder of the culture was harvested by centrifugation. New nutrient rich media was prepared, filtered, and added to the inocula. It is noted that media recycling (centrate from the centrifuge) could be done but was not standard practice. The required culture volume was then re-injected into the reactors to complete the inoculation process.

3. Thermal Model

The thermal resistance model used to depict the photobioreactor water basin is represented in Fig. S3. The water basin modeled for growth validation was not mechanically mixed but was mixed through density gradients caused by thermal effects. The approach adapted from Weyer-Geigel (1) divides the water basin to be separated into 16 equally spaced vertical nodes.

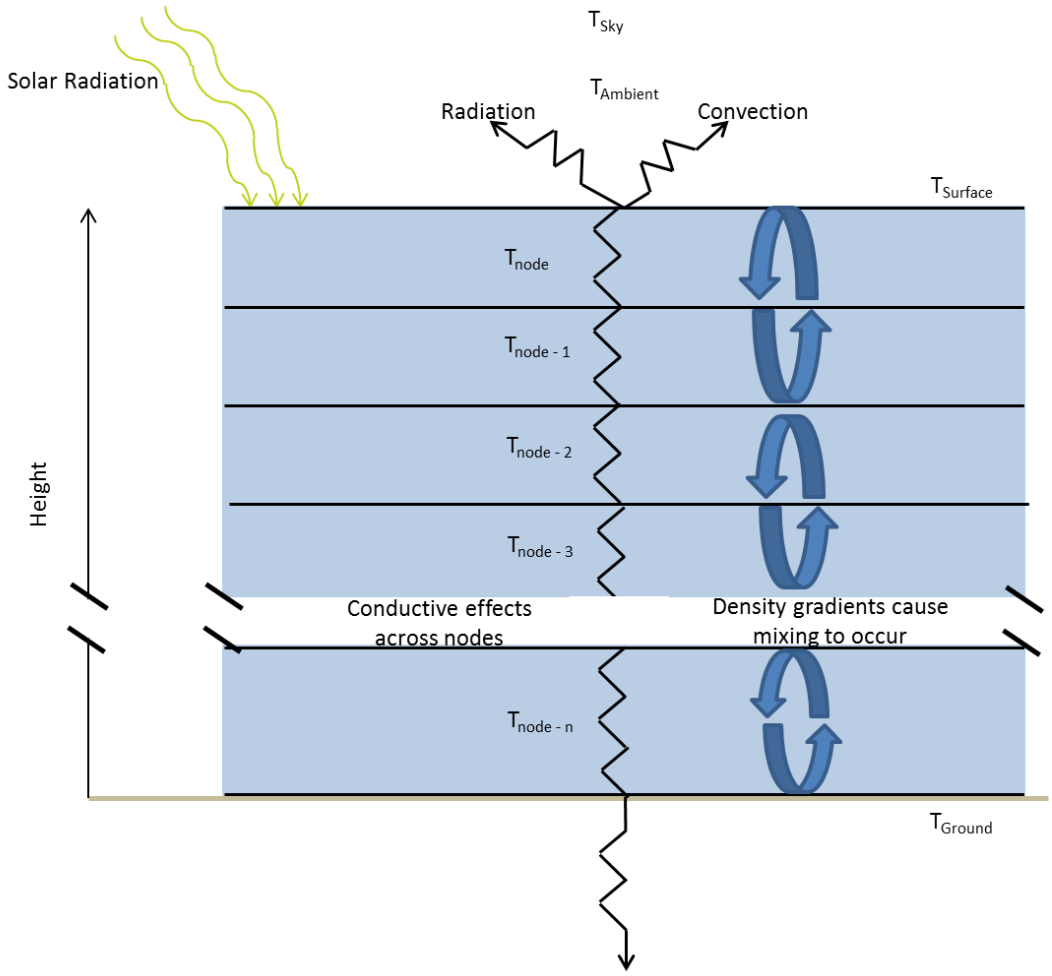

Fig. S3: Photobioreactor water basin thermal resistance model incorporated in the thermal pool model to predict the temperature at each of the 4,388 global locations.

4. Temperature Resistance Calculation

The water basin where the photobioreactors resided was separated into 16 equally spaced vertical nodes. This approach was adapted from Weyer-Geigel(1). The heat balance equation applied at each node is:

$$E_{in} - E_{out} + E_{generated} = E_{stored}$$

The heat generated in the photobioreactor is negligible and the heat balance equation for the temperature at any given internal node, n, becomes:

$$G_n - \frac{k}{L_n}(T_n - T_{n-1}) - \frac{k}{L_n}(T_n - T_{n+1}) = m_n c_p \frac{\Delta T_n}{\Delta t}$$

where G_n represents solar radiation incident at node *n*, *k* is the thermal conductivity of water, L_n is the distance between nodes, m_n is the mass of node *n*, c_p is the specific heat capacity of water, and *T* is the temperature. To represent the surface and ground node the following two equations were utilized:

$$G_{sur} - \frac{k}{L_n}(T_{sur} - T_1) - h_r\left(T_{sur} - T_{sky}\right) - h_i(T_{sur} - T_{ambient}) = \frac{m_n}{2} c_p \frac{\Delta T_{sur}}{\Delta t}$$

$$G_{bottom} - \frac{k}{L_n}(T_n - T_{n-1}) - Q_i = \frac{m_n}{2} c_p \frac{\Delta T_n}{\Delta t}$$

where G_{sur} and G_{bottom} represent the solar radiation at the surface and bottom of the reactor, respectively, h_r is the net radiation coefficient with the sky, Q_i is the stored or released energy from the ground, and h_i is the convection coefficient.

5. Growth Model

The biological growth model incorporates maximum photosynthetic rate based on a maximum carbon uptake (P_{C_max}), available photoactive radiation (PAR) (E_{av}-average PAR intensity in photobioreactor, φ_m-photon efficiency) including attenuation and losses based on Lambert-Beer absorption assumptions (α-species specific absorption coefficient), temperature efficiency (φ_T), and nitrogen efficiency ($\varphi_{qN,Xint}$) to calculate the carbon fixation rate:

$$P_C = P_{C\_max} \cdot \varphi_T \cdot \varphi_{qN,Xint} \cdot \left(1 - e^{\frac{[-\alpha \cdot \varphi_m \cdot E_{av}]}{P_{C\_max} \cdot \varphi_T \cdot \varphi_{qN,Xint}}}\right)$$

The photosynthetic productivity is a non-linear function of PAR. The model accurately captures two of the three regions of the photosynthetic productivity curve, 1) a photon flux density dominated region where the photosynthetic rate increases linearly with increasing light intensity and 2) a light saturation photosynthetic region characterized by constant photosynthetic rate with increasing PAR. The model does not include the third region, a photo-inhibition region, characterized by a decrease in photosynthetic rate with increasing photon flux based on an assumption of high culture densities and mid to low level light intensities (sunlight sourced) incident on the photobioreactors (2-5). Consistent with biological experimentation, the second region of the photosynthetic curve is effected by temperature and nitrogen efficiency terms with the initial photosynthetic slope not effected (2, 3, 6, 7).

The effect of the temperature efficiency factor on growth is illustrated through simulating the biomass growth over the course of one week in Learmonth, Australia. Temperature efficiencies of 1, 0.8, and 0.5 were simulated with biomass yields presented in Fig. S4. As expected, the maximum biomass is attained under optimum thermal conditions ($\varphi_T = 1$) with lower or higher temperatures decreasing the overall yield. Temperature indirectly affects the total lipid content in the cell through the effects on nitrogen uptake and thus does not have a linear effect on lipid productivity. Biomass results integrated with lipid modeling results yield 22.45, 20.41, and 15.62 $m^3 \cdot ha^{-1} \cdot yr^{-1}$ for the temperature

efficiency scenarios of 1, 0.8, and 0.5, respectively. For global modeling the temperature efficiency is dynamic and calculated on an hourly basis at each simulation location.

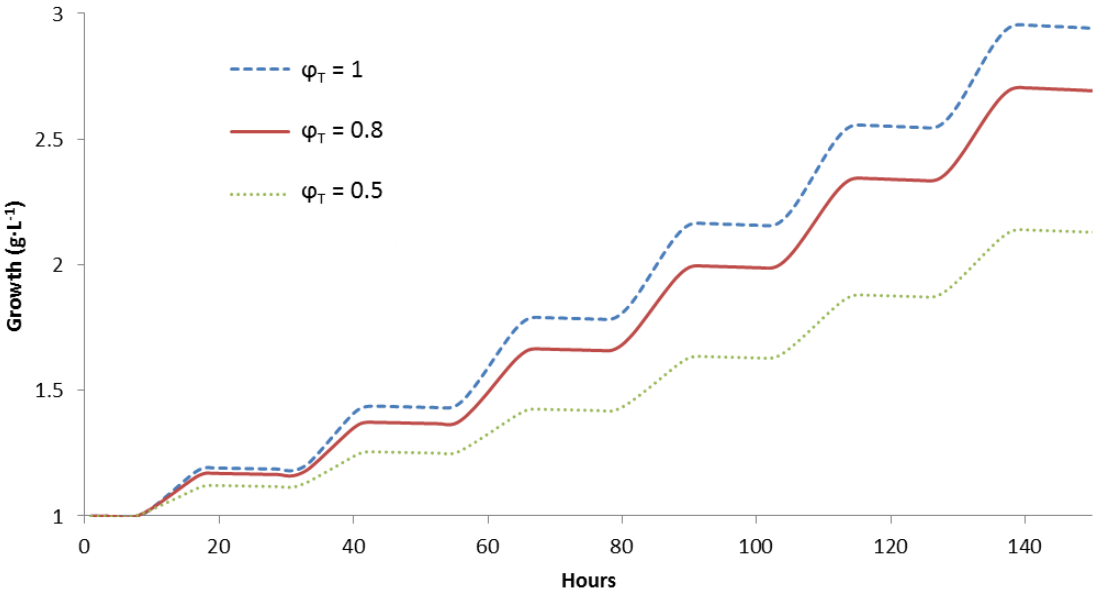

Fig. S4: Simulation of one week of growth in Learmonth, Australia with three different temperature efficiencies.

6. GIS details

The Geostatistical Analyst extension provides a suite of spatial modeling and data exploration utilities that may be used to develop surface models based on known or simulated spatial point values. This tool set facilitates the exploration and evaluation of data quality, and uses a host of surface interpolation models to develop the most appropriate spatial model for the available data. It also provides analysis methods for deterministic, geostatistical, and barrier influenced interpolation. Included within these broad categories are specific interpolation functions such as Inverse Distance Weighting, Radial Basis Functions, Kriging and CoKriging, Empirical Bayesian Kriging, and Kernel smoothing.

The Geostatistical Analyst extension requires the input of spatially explicit data with associated point values. Once the data is loaded and the appropriate associated variable identified, the utility provides a series of data evaluation screens and outputs that describe an optimal model based on the semivariogram and covariance graphs and maps. The number of lags and lag size are determined for the Ordinary Kriging model and optimization is conducted as necessary. The lag is the sample distance used to group, or bin, pairs of points and using the optimal number of lags enables scale-dependent spatial correlations (8). In the case of this analysis, and the global extent of the data the model selected an appropriate lag size of 7.3 with the correlating number of lags at 12. Manual verification of the lag value was conducted to verify the Geostatistical Analyst results.

After the appropriate analysis variables were selected, the neighborhood and sector type were evaluated. Both a standard neighborhood and smooth neighborhood type for surface interpolation were assessed. Standard neighborhood options assign weights based on distance from a specific target location assigned by the analyst. Alternatively, the smooth neighborhood function adjusts the weights using a sigmoidal function defined by a smoothing factor. Based on validation tests conducted, a smooth neighborhood type using a smoothing factor of 0.5 was selected. This produced smoother global isolines, removing excessive stair-step effects in areas of less sample data. The sector type is simply the geometry of the neighborhood in which the algorithm assesses nearby point values. The Geostatistical Analyst default of four sectors with a 45° offset was selected. Other options were tested with no measureable change in results.

7. Generated Maps

Fig. S5 represents the global map showing the 4,388 point locations that were simulated using the growth model. The standard error verifies that where the point locations are located, and indeed denser, yields a smaller error, signifying better interpolation of surface values.

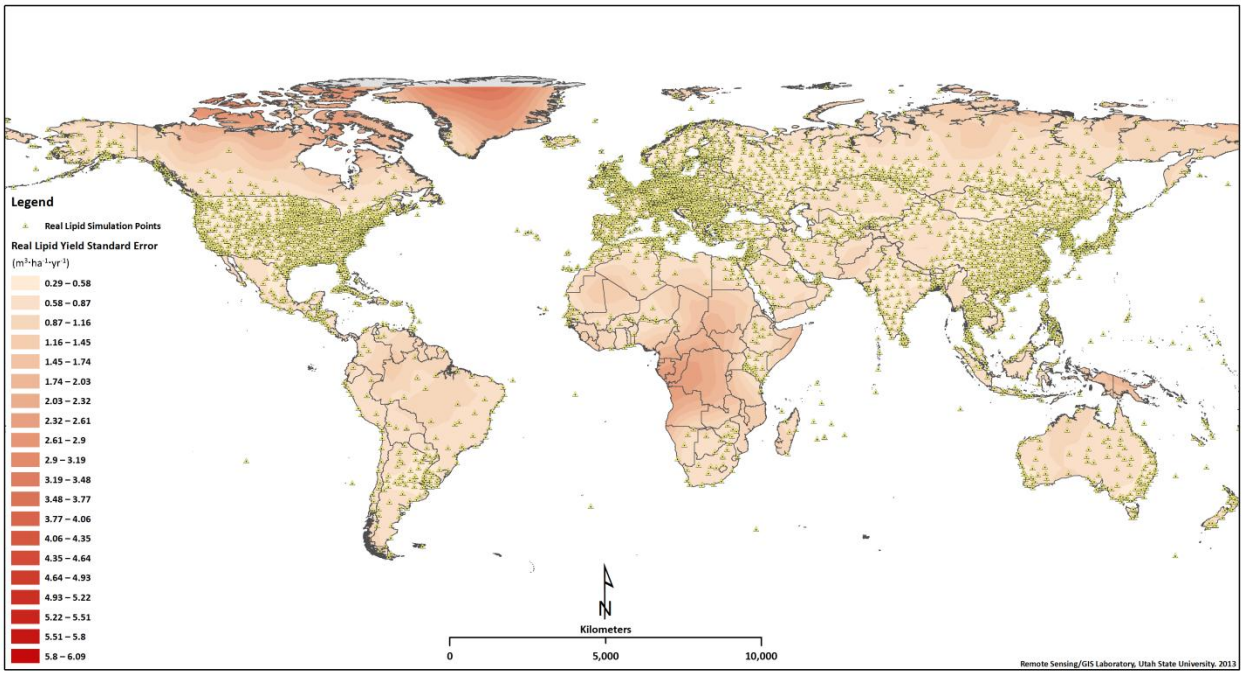

Fig. S5: Global map of the 4,388 locations coupled with standard error assessment

Fig. S6 represents the dynamic global map of the biomass productivity. A comparison between this map and the real lipid productivity map found in the paper demonstrates the non-linear relationship between lipid and biomass productivity.

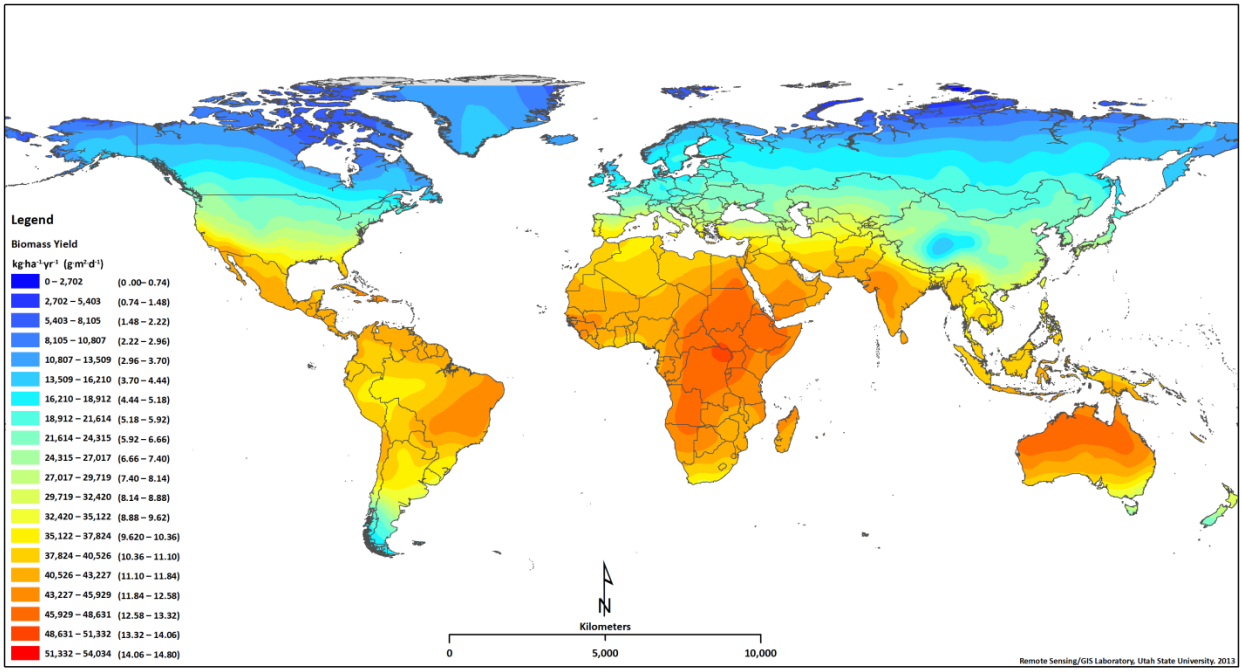

Fig. S6: World map of the biomass productivity potential from microalgae

The high, average, and low monthly lipid productivity maps are presented in Fig. S7, Fig. S8, and Fig. S9, respectively. The lipid scale for these maps ranges from 0 to 3.0 $m^3 \cdot ha^{-1} \cdot month^{-1}$ so a direct comparison can be made between the three maps. These maps do not include temporal resolution. In the northern hemisphere maximum lipid yields will be attained from May to July while in the southern hemisphere minimum lipid yields will be achieved during these months.

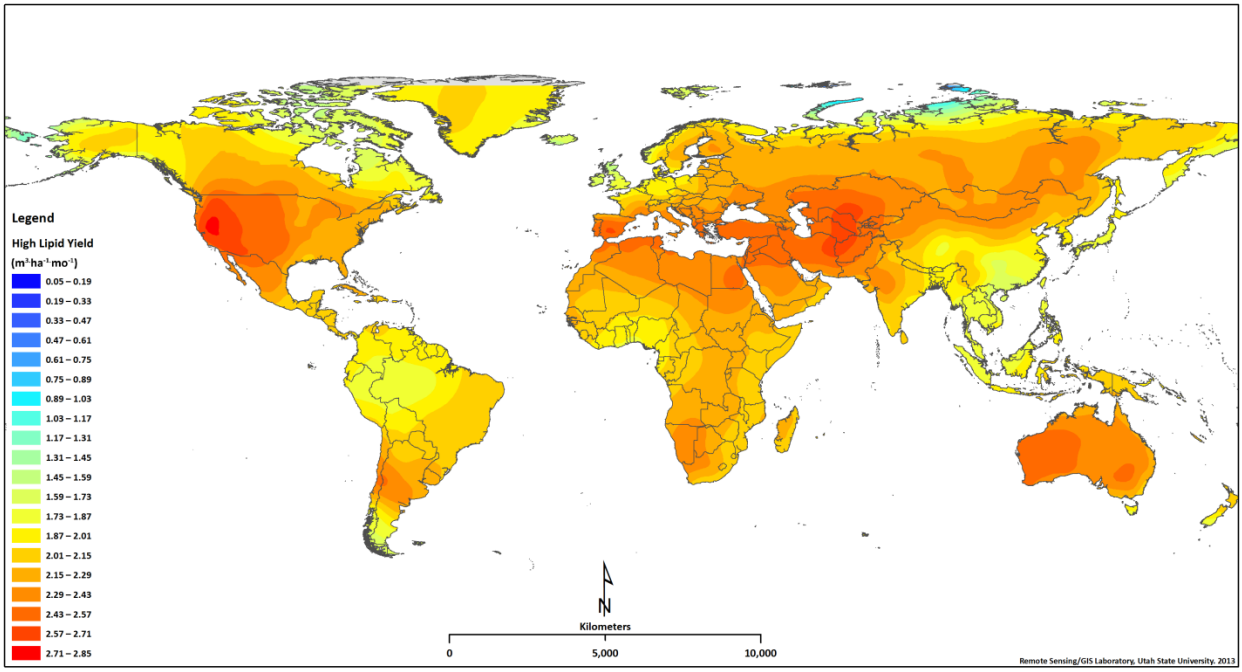

Fig. S7: Global map of the high monthly lipid productivity potential from microalgae.

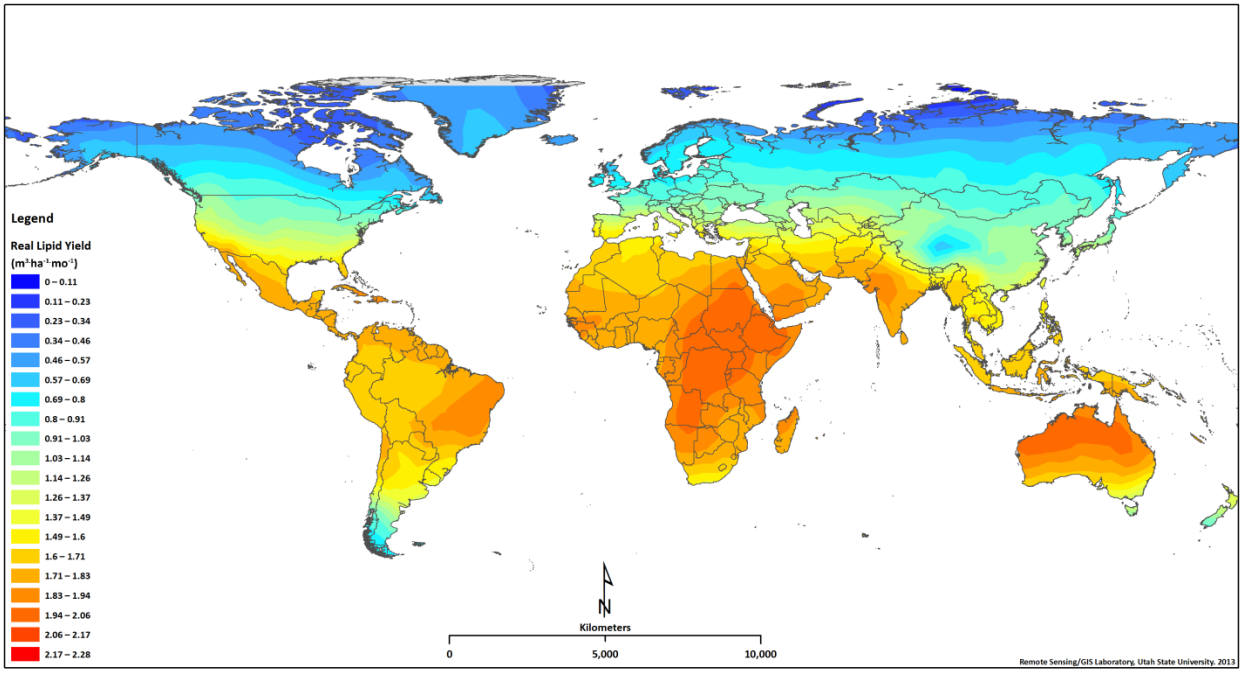

Fig. S8: Global map of the average monthly lipid productivity potential from microalgae.

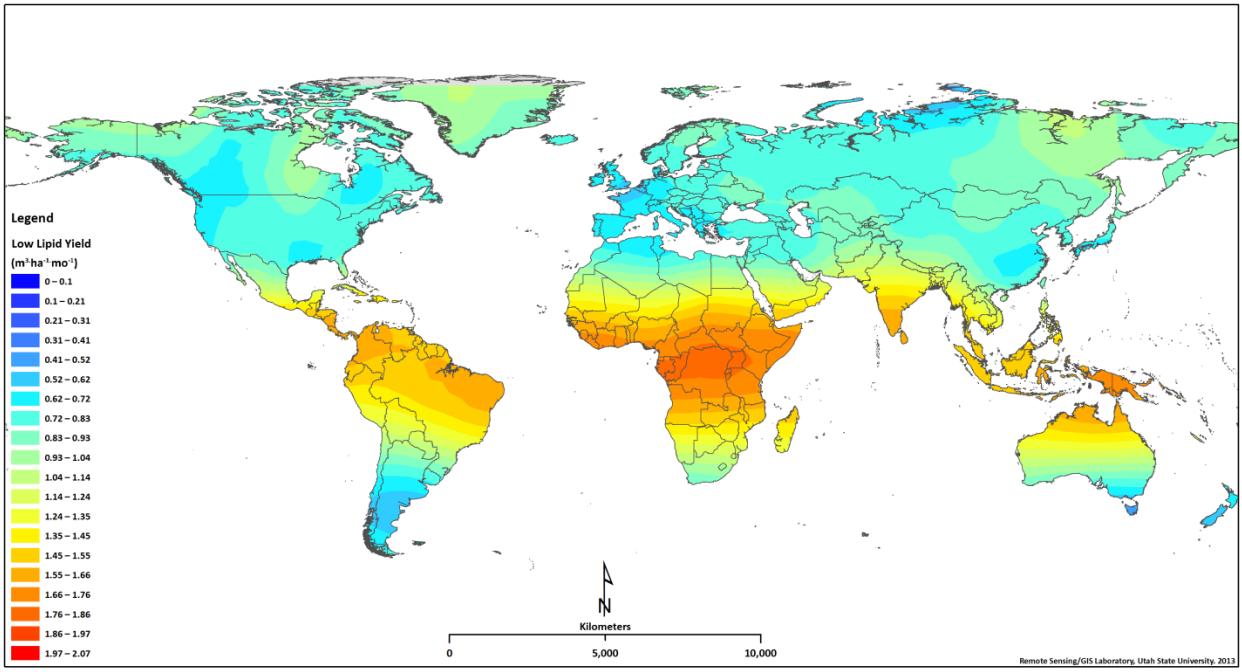

Fig. S9: Global map of the low monthly lipid productivity potential from microalgae.

8. Agricultural Land

The quantity of agricultural land available (9) and oil consumption for various regions (10) were used to evaluate the current potential impact of microalgae based biofuel on transportation fuel supplementation versus soybean based biofuel. The scalability assessment includes a 90% efficiency for the extraction of lipids from the biomass, a 90% efficiency for the conversion of oil to fuel, and a 0.8 packing factor to more accurately represent the microalgae to biofuel process at industrial scale. The amount of agricultural land required to supplement 30% of the transportation fuel consumed in each region through replacement by microalgae is directly compared to the requirements for soybean based fuels, Table S1. Assumptions for soybean yields are based on geographically based yield data and include the same efficiency assumptions for extraction and conversion as for microalgae based processing, but do not include a packing factor (11-15).

Soybean yields for different countries around the world were obtained through the United States Department of Agriculture (11). The average percentage of oil in the soybean yield was assumed at 18% (13-15) with an oil density of 923 (kg/m^3) (12). Using 90% efficiency for extraction (16), 90% efficiency for conversion (17), and a land packing factor of 0.8 (18), the amount of agricultural land required to supplement 30% of transportation oil consumption in each country was calculated.

Table S1. Amount of agricultural land needed to supplement 30% of the transportation fuel consumed for different regions around the world based on replacement by microalgae as compared to soybeans.

Location	Agricultural Land Available (hectare)	Oil Yield ($m^3 \cdot ha^{-1} \cdot yr^{-1}$)		Agricultural Land Required	
		Microalgae	Soybeans	Microalgae	Soybean
Brazil	2.35E+08	20.9	0.43	1%	66%
Canada	8.46E+07	7.0	0.50	9%	132%
China	5.09E+08	12.5	0.36	5%	160%
Japan	4.67E+06	12.6	0.23	199%	10,751%
United States	4.36E+08	12.7	0.56	8%	182%

Table S1 shows it is feasible to supplement 30% of the petroleum oil consumption of Brazil, Canada, China, and United States based on microalgae productivity potential and agricultural land. Regions such as Japan cannot practically replace their oil needs through microalgae with over 100% of their agricultural land required. Soybean requires an average of 27 times more agricultural land than microalgae in the regions examined.

9. Non-Arable Biodiesel Yields

Table S2 represents the amount of non-arable land required to supplement 30% of the transportation fuel for different countries around the world based on microalgae production. From the 56 countries represented 61% are able to supplement 30% of their transportation fuel based on non-arable land and microalgae production while 39% cannot.

Table S2: Amount of non-arable land needed to supplement 30% of oil consumption for different regions around the world based on replacement by microalgae.

Country	Lipid Productivity ($m^3 \cdot ha^{-1} \cdot yr^{-1}$)	Non-arable land (ha)	Biodiesel Produced (liters a year)	Transportation Fuel Consumption (liters a year)	Non-arable Land Required
Algeria	19.7	1.95E+08	2.49E+12	5.83E+09	0%
Argentina	16.9	9.96E+07	1.09E+12	9.84E+09	1%
Australia	22.2	2.74E+08	3.94E+12	1.63E+10	0%
Austria	10.9	4.32E+05	3.06E+09	4.33E+09	141%
Azerbaijan	14.7	1.11E+06	1.05E+10	1.47E+09	14%
Belarus	10.8	3.92E+05	2.73E+09	3.17E+09	116%
Brazil	20.9	2.06E+07	2.79E+11	4.38E+10	16%
Canada	7.0	3.62E+08	1.65E+12	3.64E+10	2%
Chile	15.2	2.78E+07	2.74E+11	6.24E+09	2%
China	12.4	2.22E+08	1.79E+12	1.90E+11	11%
Colombia	20.4	3.80E+06	5.01E+10	4.43E+09	9%
Denmark	9.1	1.51E+04	8.92E+07	2.65E+09	2,973%
Ecuador	20.2	2.25E+06	2.94E+10	3.84E+09	13%
Egypt	21.9	8.24E+07	1.17E+12	1.23E+10	1%
Finland	8.6	5.65E+05	3.13E+09	3.17E+09	101%

France	12.2	4.20E+05	3.33E+09	2.82E+10	848%
Germany	9.9	2.16E+05	1.38E+09	3.89E+10	2,824%
Greece	16.9	6.20E+03	6.80E+07	5.37E+09	7,900%
India	20.4	6.08E+06	8.04E+10	5.99E+10	74%
Indonesia	20.3	4.18E+06	5.51E+10	2.50E+10	45%
Iran	19.0	1.18E+08	1.45E+12	3.13E+10	2%
Ireland	9.1	2.00E+03	1.18E+07	2.16E+09	18,376%
Israel	20.7	1.12E+06	1.50E+10	4.74E+09	32%
Italy	14.7	7.86E+05	7.48E+09	2.24E+10	299%
Japan	12.6	9.16E+04	7.49E+08	7.61E+10	10,165%
Kazakhstan	12.3	2.03E+08	1.62E+12	4.47E+09	0%
Kuwait	21.1	1.44E+06	1.97E+10	7.29E+09	37%
Lithuania	10.4	8.98E+04	6.05E+08	9.07E+08	150%
Malaysia	19.8	7.06E+04	9.05E+08	1.04E+10	1,149%
Mexico	20.8	1.18E+07	1.59E+11	3.23E+10	20%
New Zealand	14.2	9.59E+05	8.80E+09	2.44E+09	28%
Norway	6.6	1.67E+07	7.11E+10	3.77E+09	5%
Pakistan	20.1	2.70E+07	3.51E+11	6.98E+09	2%
Peru	19.5	1.65E+07	2.09E+11	3.35E+09	2%
Philippines	19.2	3.16E+05	3.92E+09	4.53E+09	116%
Poland	10.2	6.08E+05	4.02E+09	8.76E+09	218%
Portugal	17.6	1.43E+05	1.63E+09	3.80E+09	233%
Qatar	21.2	9.50E+05	1.31E+10	2.79E+09	21%
Romania	12.4	6.49E+04	5.22E+08	3.07E+09	588%
Russian Federation	7.8	2.41E+08	1.22E+12	5.15E+10	4%
Saudi Arabia	21.5	1.67E+08	2.33E+12	4.52E+10	2%
Slovakia	11.3	9.40E+03	6.87E+07	1.22E+09	1,777%
South Africa	20.1	1.63E+07	2.13E+11	9.38E+09	4%
South Korea	12.9	2.91E+04	2.43E+08	3.80E+10	15,588%
Spain	16.3	7.70E+05	8.12E+09	2.23E+10	274%
Sweden	8.6	2.82E+06	1.56E+10	4.81E+09	31%
Switzerland	11.1	4.67E+05	3.35E+09	3.91E+09	117%
Thailand	19.0	4.65E+04	5.71E+08	1.83E+10	3,200%
Trinidad and Tobago	20.9	1.50E+03	2.03E+07	5.58E+08	2,743%
Turkey	15.9	6.55E+06	6.74E+10	1.10E+10	16%
Turkmenistan	16.7	3.55E+07	3.85E+11	1.67E+09	0%
Ukraine	11.9	1.37E+06	1.06E+10	4.60E+09	44%
United Arab Emirates	21.5	6.11E+06	8.51E+10	1.14E+10	13%
United States	12.7	7.03E+07	5.80E+11	2.86E+11	49%
Uzbekistan	15.6	3.05E+07	3.09E+11	1.36E+09	0%
Venezuela	21.0	2.51E+06	3.42E+10	1.28E+10	37%

A number of countries around the world have implemented biodiesel goals. Brazil, China, and United States have biodiesel goals (by the years 2013, 2020, and 2030 respectively) of 7.30E+09, 1.40E+11, and 2.86E+11 liters per year respectively (1, 19, 20). Using the same efficiencies and packing factors as the previous scalability assessments, the amount of non-arable land required in Brazil, China, and United States to meet each respective biodiesel volume goal is 3%, 8%, and 49%, respectively. It is feasible for these three countries to achieve their biodiesel goals through microalgae and non-arable land use. Non-arable land utilization for microalgae production provides a benefit over traditional terrestrial crops such as soy which compete with food crops for agricultural land.

10. Literature

The literature survey performed was an effort to compare the current near-term large scale lipid productivity potential of microalgae results from this study to the results found in literature. Table S3 represents the literature source with its respective oil yield along with the assumptions made to convert the result of oil yield to $m^3 \cdot ha^{-1} \cdot yr^{-1}$. The lipid productivity potential of microalgae from this study shows that literature is dramatically overestimating the lipid productivity potential of microalgae.

Table S3: Table comparing reported productivity potentials (some calculations performed for comparison purposes with assumptions detailed in notes column) from various sources.

Source	Oil Yield ($m^3.ha^{-1}.yr^{-1}$)	Article Type	Purpose of Scaling	Notes
Ramachandra et al. (21)	2.3	Research-Data	Microalgae Potential	8.8-24.6% oil, , p=860kg m^{-3}, Wastewater
Pate RC (22)	4.7	Research-Model	Modeling Effort	
Lam et al. (23)	5.2	Review	Microalgae Potential	30% oil, p=860kg m^{-3}
Resurreccion et al. (24)	5.5	Research-Model	LCA-Modeling Effort	13.4-32.4% oil, p=860kg m^{-3}, ORP, PBR
Quinn et al. (25)	7.04	Research-Data	Microalgae Potential	Growth Data, PBR
Ramachandra et al. (21)	7.6	Research-Data	Microalgae Potential	8.8-24.6% oil, p=860kg m^{-3}, Wastewater
Scott et al. (26)	8.4	Review	Microalgae Potential	50% oil, p=860kg m^{-3}
Lam et al. (23)	8.7	Review	Microalgae Potential	30% oil, p=860kg m^{-3}
Vasudevan et al. (27)	9.0	Research-Model	LCA-Modeling Effort	ORP
Clarens et al. (28)	9.7	Research-Model	Economic-Modeling Effort	assumed 30% oil and p=860kg m^{-3}, ORP
Moheimani NR (29)	10.0	Research-Data	Microalgae Potential	27% oil, p=860kg m^{-3}, Growth Data, PBR
Guieysse et al. (30)	11.8	Research-Model	Modeling Effort	25% oil, 11.1-25.7 g m^{-2} day^{-1}, ORP
Clarens et al. (28)	11.8	Research-Model	Economic-Modeling Effort	assumed 30% oil and p=860kg m^{-3}, ORP
Schenk et al. (31)	12.5	Review	Microalgae Potential	10 - 50 g m^{-2} d^{-1}, 30 - 50% TAG
Moheimani NR (29)	12.7	Research-Data	Microalgae Potential	27% oil, p=860kg m^{-3}, Growth Data, PBR
ANL;NREL;PNNL (32)	13.1	Research-Model	Harmonization Modeling	25% oil, p=920kg m^{-3}, 13.2g m^{-1} day^{-1}
Campbell et al. (33)	19.1	Research-Model	LCA-Modeling Effort	15 - 30 g m^{-2} d^{-1}, 30% oil, p=860kg m^{-3}, ORP
Lardon et al. (34)	19.3	Research-Model	LCA-Modeling Effort	18.4 - 39.2% oil, 24.8 - 19.3 g m^{-2} d^{-1}, ORP
Vasudevan et al. (27)	20.0	Research-Model	LCA-Modeling Effort	ORP
Rodolfi et al. (35)	21.1	Research-Model	Economic-Modeling Effort	20-30 ton ha^{-1} yr^{-1}, p=860kg m^{-3}, PBR
Quinn et al. (25)	21.1	Research-Data	Microalgae Potential	Growth Data, PBR
Chisti et al. (36)	21.2	Letter Response	Microalgae Potential	25 g m^{-2} d^{-1}, 20% - 50% oil, ORP
Davis et al. (37)	24.0	Research-Model	Economic-Modeling Effort	25% oil, 25 g m^{-2} d^{-1}, ρ=860kg m^{-3}, ORP

Guieysse et al. (30)	27.3	Research-Model	Modeling Effort	25% oil, 11.1-25.7 g m^{-2} day^{-1}, ORP
Resurreccion et al. (24)	30.3	Research-Model	LCA-Modeling Effort	13.4-32.4% oil, p=860kg m^{-3}, ORP, PBR
Rodolfi et al. (35)	31.6	Research-Model	Economic-Modeling Effort	20-30 ton ha^{-1} yr^{-1}, p=860kg m^{-3}, PBR
Lardon et al. (34)	32.1	Research-Model	LCA-Modeling Effort	18.4 - 39.2% oil, 24.8 - 19.3 g m^{-2} d^{-1}, ORP
Scott et al. (26)	34.9	Review	Microalgae Potential	50% oil, p=860kg m^{-3}
Campbell et al. (33)	38.2	Research-Model	LCA-Modeling Effort	15 - 30 g m^{-2} d^{-1}, 30% oil, ORP
Wijffels and Barbosa (38)	40.0	Perspective	Microalgae Potential	3% solar efficiency, 50% oil
Williams and Laurens (39)	41.6	Review	Economic-Modeling Effort	35% oil, 28 g m^{-2} d^{-1}, p=860kg m^{-3}
Yeang (40)	46.0	Opinion	Microalgae Potential	4.6 l m^{-2} yr^{-1}, PBR
Batan et al. (18)	53.1	Research-Model	LCA-Modeling Effort	50% oil, 25 g m^{-2} d^{-1}, p=860kg m^{-3}, PBR
Chisti et al. (36)	53.1	Letter Response	Microalgae Potential	25 g m^{-2} d^{-1}, 20% - 50% oil, ORP
Mata et al. (15)	58.7	Review	Microalgae Potential	30 - 70% oil
Chisti et al. (41)	58.7	Review	Microalgae Potential	30% oil, PBR
Liao et al. (42)	59.4	Research-Model	LCA-Modeling Effort	40% oil, p=860kg m^{-3}, ORP
Pate RC (22)	60.8	Research-Model	Modeling Effort	
Chisti et al. (43)	98.4	Opinion	Microalgae Potential	30% oil, 1.535 kg m^{-3} d^{-1}
Schenk et al. (31)	98.5	Review	Microalgae Potential	10 - 50 g m^{-2} d^{-1}, 30 - 50% TAG
Mata et al. (15)	136.9	Review	Microalgae Potential	30 - 70% oil

Some authors reported a range of productivity potential
[a] The low values are repeated in this table
[b] The high values are repeated in this table

11. Nomenclature

Symbol	Description	Unit
Ea	activation energy carboxylation Rubisco	$J \cdot mol^{-1}$
E_{av}	average light intensity in photobioreactor	$\mu mol \cdot m^{-2} \cdot s^{-1}$
P_c	photosynthetic rate (carbon)	h^{-1}
P_{c_max}	maximum photosynthetic rate (carbon)	h^{-1}
R	universal gas constant	$J \cdot K^{-1} \cdot mol^{-1}$
rR_c	maintenance respiration rate (carbon)	h^{-1}
T	bath temperature	°C
T_{opt}	optimum growth temperature	°C
α	absorption coefficient	$m^2 \cdot g^{-1}$
μ	carbon specific growth rate	h^{-1}
φ_m	photon efficiency	$g \cdot (\mu mol\ photons)^{-1}$
$\varphi_{qN,X\ int}$	uptake of internal nitrogen concentration efficiency	-
φ_T	temperature efficiency factor	-
Ψ	biosynthetic energy required for nitrogen uptake	h^{-1}

References

1. Quinn JC, Catton K, Wagner N, Bradley TH (2012) Current large-scale US biofuel potential from microalgae cultivated in photobioreactors. *BioEnergy Res* 5(1):49-60.
2. Henley WJ (1993) Measurement and interpretation of photosynthetic light-response curves in algae in the context of photoinhibition and diel changes. *J Phycol* 29(6):729-739.
3. MacIntyre HL, Kana TM, Anning T, Geider RJ (2002) Photoacclimation of photosynthesis irradiance response curves and photosynthetic pigments in microalgae and cyanobacteria. *J Phycol* 38(1):17-38.
4. Richmond A (2000) Microalgal biotechnology at the turn of the millennium: A personal view. *J Appl Phycol* 12(3-5):441-451.
5. Goldman JC (1979) Outdoor algal mass-cultures. 2. Photosynthetic yield limitations. *Water Res* 13(2):119-136.
6. Ihnken S, Eggert A, Beardall J (2010) Exposure times in rapid light curves affect photosynthetic parameters in algae. *Aquat Bot* 93(3):185-194.
7. Furuya K, Hasegawa O, Yoshikawa T, Taguchi S (1998) Photosynthesis-irradiance relationship of phytoplankton and primary production in the vicinity of Kuroshio warm core ring in spring. *Journal of Oceanography* 54(5):545-552.
8. ArcGIS 10.2 for server functionality matrix (2013) Esri (Environmental Systems Research Institute) http://www.esri.com/library/brochures/pdfs/arcgis-server-functionality-matrix.pdf Accessed October 2013.
9. Land area (2013) The World Bank http://data.worldbank.org/indicator/AG.LND.TOTL.K2 Accessed July 2013.
10. BP statistical review of world energy June 2013 (2013) British Petroleum http://www.bp.com/content/dam/bp/pdf/statistical-review/statistical_review_of_world_energy_2013.pdf Accessed July 2013.
11. World Agricultural Production (2005) United States Department of Agriculture Foreign Agricultural Service http://www.fas.usda.gov/wap/circular/2005/05-08/tables.html Accessed August 2013.
12. Rojas EEG, Coimbra JSR, Telis-Romero J (2013) Thermophysical properties of cotton, canola, sunflower and soybean oils as a function of temperature. *Int J Food Prop* 16(7):1620-1629.
13. Panichelli L, Dauriat A, Gnansounou E (2009) Life cycle assessment of soybean-based biodiesel in Argentina for export. *Int J Life Cycle Assess* 14(2):144-159.
14. Hou J, Zhang PD, Yuan XZ, Zheng YH (2011) Life cycle assessment of biodiesel from soybean, jatropha and microalgae in China conditions. *Renew Sust Energ Rev* 15(9):5081-5091.
15. Mata TM, Martins AA, Caetano NS (2010) Microalgae for biodiesel production and other applications: a review. *Renew Sust Energ Rev* 14(1):217-232.
16. Frank E, Han J, Palou-Rivera I, Elgowainy A, Wang M (2011) Life-cycle analysis of algal lipid fuels with the GREET model.
17. Khoo HH, et al. (2011) Life cycle energy and CO2 analysis of microalgae-to-biodiesel: preliminary results and comparisons. *Bioresour Technol* 102(10):5800-5807.
18. Batan L, Quinn J, Willson B, Bradley T (2010) Net energy and greenhouse gas emission evaluation of biodiesel derived from microalgae. *Environ Sci Technol* 44(20):7975-7980.
19. Timilsina G, R., Shrestha A (2010) Policy Research Working Paper 5364.

20. Nass LL, Pereira PAA, Ellis D (2007) Biofuels in Brazil: An overview. *Crop Science* 47(6):2228-2237.
21. Ramachandra TV, Madhab MD, Shilpi S, Joshi NV (2013) Algal biofuel from urban wastewater in India: Scope and challenges. *Renew Sust Energ Rev* 21:767-777.
22. Pate RC (2013) Resource requirements for the large-scale production of algal biofuels. *Biofuels* 4(4):409-435.
23. Lam MK, Lee KT (2012) Microalgae biofuels: A critical review of issues, problems and the way forward. *Biotechnol Adv* 30(3):673-690.
24. Resurreccion EP, Colosi LM, White MA, Clarens AF (2012) Comparison of algae cultivation methods for bioenergy production using a combined life cycle assessment and life cycle costing approach. *Bioresour Technol* 126:298-306.
25. Quinn JC, et al. (2012) *Nannochloropsis* production metrics in a scalable outdoor photobioreactor for commercial applications. *Bioresour Technol* 117:164-171.
26. Scott SA, et al. (2010) Biodiesel from algae: Challenges and prospects. *Curr Opin Biotechnol* 21(3):277-286.
27. Vasudevan V, et al. (2012) Environmental performance of algal biofuel technology options. *Environ Sci Technol* 46(4):2451-2459.
28. Clarens AF, Resurreccion EP, White MA, Colosi LM (2010) Environmental life cycle comparison of algae to other bioenergy feedstocks. *Environ Sci Technol* 44(5):1813-1819.
29. Moheimani NR (2013) Long-term outdoor growth and lipid productivity of *Tetraselmis suecica*, *Dunaliella tertiolecta* and *Chlorella sp* (Chlorophyta) in bag photobioreactors. *J Appl Phycol* 25(1):167-176.
30. Guieysse B, Bechet Q, Shilton A (2013) Variability and uncertainty in water demand and water footprint assessments of fresh algae cultivation based on case studies from five climatic regions. *Bioresour Technol* 128:317-323.
31. Schenk PM, et al. (2008) Second generation biofuels: High-efficiency microalgae for biodiesel production. *BioEnergy Res* 1(1):20-43.
32. ANL, NREL, PNNL (2012) Renewable diesel from algal lipids: An integrated baseline for cost, emissions, and resource potential from a harmonized model. in *ANL/ESD/12-4; NREL/TP-5100-55431; PNNL-21437* (Argonne, IL: Argonne National Laboratory; Golden, CO: National Renewable Energy Laboratory; Richland, WA: Pacific Northwest National Laboratory).
33. Campbell PK, Beer T, Batten D (2011) Life cycle assessment of biodiesel production from microalgae in ponds. *Bioresour Technol* 102(1):50-56.
34. Lardon L, Helias A, Sialve B, Steyer JP, Bernard O (2009) Life-cycle assessment of biodiesel production from microalgae. *Environ Sci Technol* 43(17):6475-6481.
35. Rodolfi L, et al. (2009) Microalgae for oil: Strain selection, induction of lipid synthesis and outdoor mass cultivation in a low-cost photobioreactor. *Biotechnol Bioeng* 102(1):100-112.
36. Chisti Y (2008) Response to Reijnders: Do biofuels from microalgae beat biofuels from terrestrial plants? *Trends Biotechnol* 26(7):351-352.
37. Davis R, Aden A, Pienkos PT (2011) Techno-economic analysis of autotrophic microalgae for fuel production. *Appl Energy* 88(10):3524-3531.
38. Wijffels RH, Barbosa MJ (2010) An outlook on microalgal biofuels. *Science* 329(5993):796-799.
39. Williams PJL, Laurens LML (2010) Microalgae as biodiesel & biomass feedstocks: Review & analysis of the biochemistry, energetics & economics. *Energy Environ Sci* 3(5):554-590.
40. Yeang K (2008) Biofuel from algae. *Archit Des* (193):118-119.
41. Chisti Y (2007) Biodiesel from microalgae. *Biotechnol Adv* 25(3):294-306.
42. Liao YF, Huang ZH, Ma XQ (2012) Energy analysis and environmental impacts of microalgal biodiesel in China. *Energy Policy* 45:142-151.

43. Chisti Y (2008) Biodiesel from microalgae beats bioethanol. *Trends Biotechnol* 26(3):126-131.